Applied Catalysis B: Environmental 232 (2018) 205–212

Contents lists available at ScienceDirect

Applied Catalysis B: Environmental

journal homepage: www.elsevier.com/locate/apcatb

Revealing structure-activity relationships in chromium free high temperature shift catalysts promoted by earth abundant elements

Minghui Zhu[a], Özgen Yalçın[a,b], Israel E. Wachs[a,*]

[a] Operando Molecular Spectroscopy & Catalysis Laboratory, Department of Chemical and Biomolecular Engineering, Lehigh University, Bethlehem, PA 18015 USA
[b] Department of Chemical Engineering, Middle East Technical University, Ankara 06800, Turkey

ARTICLE INFO

Keywords:
Water-gas shift
High temperature
Promoters
Iron-based catalysts
Cr-free

ABSTRACT

Finding a replacement for the toxic hexavalent chromium oxide in commercial iron oxide-based high temperature water-gas shift (HT-WGS) catalyst is of current environmental concern. Previous studies in developing Cr-free catalysts mainly focus on ex-situ characterization on catalysts bulk structure. In the present study, CuO/MO_x-Fe_2O_3 catalysts promoted by Si, Al, Cr or Mg were studied with XRD, *in situ* Raman, HS-LEIS, BET, transient $C^{16}O_2 \rightarrow C^{18}O_2$ isotopic switch, steady-state WGS activity test and CO-TPR to elucidate their structure-activity relationships. The Mg and Al are homogeneously distributed within both fresh and activated catalysts as texture promoters, while the Si exists as discrete SiO_2 that is covered by iron oxides. During the HT-WGS reaction, the Mg promoter resulted in the poorest thermally stability and least amount of metal-metal oxide interface, and the Si promoter inhibited the reducibility of surface oxygen. Only the Al promoter was found to yield a catalyst that possessed similar catalyst structure, comparable thermostability and activity with the Cr-promoted catalyst. This work demonstrates the importance of *in situ* characterization to the rational design of Cr-free iron oxide based HT-WGS catalysts.

1. Introduction

Industrial H_2 is currently primarily produced by methane steam reforming (MSR) followed by the water-gas shift (WGS) reaction ($CO + H_2O \leftrightarrow CO_2 + H_2$) to control the H_2-to-CO ratio. The WGS reaction involves the interaction of carbon monoxide with steam to produce H_2 and CO_2 and is commercially performed in several temperature stages with different catalysts to optimize both the reaction rate and CO conversion [1–3]. The high temperature water-gas shift (HT-WGS) reaction is commercially performed at ~350–450 °C with iron oxide-based catalysts and the low temperature water-gas shift (LT-WGS) reaction is commercially performed at ~190–250 °C with supported copper-based catalysts.

During the HT-WGS reaction, the catalytic active phase is magnetite (Fe_3O_4), which is prone to deactivate due to sintering and over-reduction [4–6]. Chromium oxide is added as textural promoter to stabilize the surface area and prevent over-reduction of the magnetite as well [7]. Copper is also added as a promoter to increase the catalytic activity and allow wider operating temperature range [8–12]. Recent study shows that copper functions as a chemical promoter by providing new highly active catalytic active metallic Cu° sites and Cu-iron oxide interfacial sites [13].

A major concern about the current HT-WGS iron-chromium oxide-based catalyst is the presence of hexavalent chromium (Cr^{+6}), a potent carcinogen that threatens human life and the environment [14]. This issue has motivated intensive research over the past decades to develop Cr-free HT-WGS catalysts that possess comparable performance to the current Cu promoted iron-chromium oxide catalyst. Rethwisch and Dumesic examined the HT-WGS activity of Zn and Mg promoted magnetite (Fe_3O_4) and only achieved lower activity than iron-chromium oxide catalysts [15]. Chinchen was the first to investigate Cu promoted iron oxide catalysts containing Ca, Ce and Zr oxides that form bulk spinel mixed oxide compounds [16]. Lee et al. have done extensive research on Ni-promoted iron oxide catalysts and found that incorporation of Ni to a Cu promoted iron oxide catalyst increased CO conversion by increasing the surface area of the catalysts [17–19]. Recently, aluminum has received more attention as Cr replacement for Cu promoted iron oxide catalysts without compromising the catalytic performance [20–22]. Those studies, unfortunately, mainly focused on bulk structure of the catalysts before the WGS reaction with a lack of *in situ* characterization during the reaction which is essential to fully understand the structure-property relationships of those Cr-free iron oxide-based HT-WGS catalysts [23–29].

In this work, we sought to understand the bulk/surface structure of

* Corresponding author.
E-mail address: iew0@lehigh.edu (I.E. Wachs).

https://doi.org/10.1016/j.apcatb.2018.03.051
Received 5 December 2017; Received in revised form 21 January 2018; Accepted 17 March 2018
Available online 19 March 2018
0926-3373/

a series of ternary copper promoted iron oxide based catalysts before and during reaction. Three widely accessible earth abundant elements: Mg, Al and Si were selected as Cr substitution. The bulk structures of catalysts were characterized by XRD and *in situ* Raman spectroscopy. The top-most surface of the catalysts was characterized by High Sensitivity-Low Energy Ion Scattering (HS-LEIS) spectroscopy. Their catalytic performance for HT-WGS was evaluated by steady-state reaction and CO-TPR. The current findings provide fundamental insights into those Cr free iron oxide based catalysts and can guide the rational design of further improved catalysts.

2. Experimental section

2.1. Catalyst synthesis

The binary SiO_2-Fe_2O_3, MgO-Fe_2O_3, Al_2O_3-Fe_2O_3 and Cr_2O_3-Fe_2O_3 mixed oxide catalysts were synthesized using an ammonia assisted co-precipitation method. The employed precursors were iron nitrate (Sigma Aldrich, 99.999% trace metals basis), tetraethyl orthosilicate (Sigma Aldrich, 99.999% trace metals basis), magnesium nitrate (Sigma Aldrich, 99.999% trace metals basis), aluminum nitrate (Sigma Aldrich, 99.997% trace metals basis) and chromium nitrate (Sigma Aldrich, 99.99% trace metals basis). Calculated amounts of metal precursors were mixed and dissolved in deionized water. Dilute aqueous ammonia was added dropwise to the solution to achieve desired pH. The dark brown precipitate formed was aged overnight and filtered off, oven-dried at 80 °C for 12 h and subsequently calcined at 400 °C for 3 h in static air. Those catalysts contain 8 wt.% of promoters in the oxidized form. The ternary Cu-promoted catalysts were further synthesized by incipient-wetness impregnation of aqueous solution of copper (II) nitrate (Sigma Aldrich, 99.99% trace metals basis) to introduce CuO with a loading of 3 wt.%.

2.2. BET surface area measurement

The surface areas of both fresh and used catalysts were measured by a 3-point flow BET method with an Altamira Instruments system (AMI-200) equipped with a TCD detector. The N_2 adsorption/desorption amount were measured at three different partial pressures (P/P_0 = 0.14, 0.22 and 0.30) for the calculation of surface areas. Prior to the measurement, the fresh samples were heated at ~150 °C in flowing He to remove any adsorbed impurities. To measure BET surface areas of activated sample, the reactor was flushed with He after the HT-WGS reaction and quenched with liquid nitrogen without exposing the pyrophoric catalyst to air (*in situ* BET).

2.3. X-ray diffraction (XRD) spectroscopy

Powder X-ray diffraction (XRD) patterns of fresh WGS catalysts were measured on a Rigaku Miniflex II diffractometer using Cu K-α radiation (1.5418 Å). Full scans from 10 to 80° (2-theta) were performed with a scan rate of 1°/min. Additionally, the major XRD peak from the hematite phase at 34.5–37.5° was scanned with a rate of 0.1°/min to obtain better peak resolution.

2.4. In situ Raman spectroscopy

The *in situ* Raman spectra were collected with a Horiba LabRam-HR spectrometer equipped with a confocal microscope, 2400/900 grooves/mm gratings, and a notch filter. The visible laser excitation at 442 nm (violet) was generated by a He-Cd laser. The lasers were focused on the samples with a confocal microscope equipped with a 50× long working distance objective (Olympus BX-30- LWD). And the scattered photons were directed and focused onto a single-stage monochromator and measured with a UV-sensitive LN2-cooled CCD detector (Horiba CCD-3000 V). Catalysts were placed in a high-temperature reactor cell (Linkam CCR1000) with a temperature controller (Linkam TMS94). Spectrum of the dehydrated samples was collected after a 1-h heating treatment at 400 °C under 10% O_2/Ar (Airgas, certified, 10% O_2/Ar balance) to remove any possibly adsorbed organic impurities and moisture. For *in situ* spectrum of the activated catalysts during RWGS reaction, dehydrated catalysts were further treated with a mixture of 10 ml/min CO_2 (Airgas, UHP certified gas), 10 ml/min H_2 (Airgas, UHP certified gas) and 10 ml/min Ar (Airgas, UHP certified gas)) for 1 h.

2.5. High-sensitivity low-energy ion scattering (HS-LEIS) spectroscopy

The outermost surface layer of samples was analyzed by HS-LEIS (ION-TOF Qtac^{100}) equipped with a highly sensitive double toroidal analyzer. Prior to the measurements, samples were cleaned with oxygen plasma for 30 min in a preparation chamber connected to the spectrometer to remove any possibly adsorbed impurities. To characterize catalyst surface after RWGS reaction, previously cleaned samples were treated under a static reaction mixture (~100 mbar CO_2 and ~100 mbar H_2) at 400 °C for 1 h. The activated catalysts were then transferred into the measurement chamber in vacuum to prevent the re-oxidation by air. Two different probing ions were used: 1) 3 keV He^+ as ion sources and sputtered with 0.5 keV Ar^+, each sputter and measurement cycle yields a total of 2×10^{14} ions/cm^2 and 2) 5 keV Ne^+ as ion sources and sputtered with 0.5 keV Ar^+, each sputter and measurement cycle yields a total of approximately 1.1×10^{15} ions/cm^2. Each total dose of 1×10^{15} ions/cm^2 corresponds to ~1 atomic layer [30].

2.6. Isotope switch experiments

The $C^{16}O_2/C^{18}O_2$ isotope switch experiments were carried out with an Altamira Instruments system (AMI-200) connected to Dymaxion Dycor mass spectrometer (DME200MS). Approximately 20 mg of catalyst was loaded into a quartz U-tube and initially dehydrated with 10% O_2/Ar at 400 °C to remove any residual carbonaceous residue and moisture. After dehydration, the catalyst was first equilibrated in the flowing $C^{16}O_2/H_2$ RWGS reaction conditions at 330 °C for 60 minutes, then flushed with inert He (20 ml/min He) for 10 min to remove residual $C^{16}O_2/H_2$ reactants from the system, and lastly exposed to a flow of isotopic labelled $C^{18}O_2/H_2$ reaction mixture (10 ml/min $C^{18}O_2$, 10 ml/min H_2). The time-resolved reaction products were monitored every 0.5 s with the online mass spectrometer (MS).

2.7. Steady-state HT-WGS reaction

The steady-state HT-WGS reaction was performed on an Altamira AMI-200 instrument equipped with a Dycor Dymaxion DME200MS online quadrupole mass spectrometer. Approximately 10 mg of catalyst was loaded into a U-type quartz tube and held in place by quartz wool. After initial dehydration under 10% O_2/Ar at 400 °C for 1 h, the catalyst was flushed with He for 10 min, after which the reaction mixture was introduced (10 ml/min 10% CO/Ar, 10 ml/min He and water vapor introduced by flowing the gas through a water bubbler at 25 °C to carry 2.5 vol. % water vapor). The HT-WGS reaction was performed at different temperatures for 90 min for steady-state operations. The following m/z were observed: H_2, m/z = 2; H_2O, m/z = 18; CO (corrected from CO_2 cracking), m/z = 28; CO_2, m/z = 44.

The turnover frequency (TOF) values for the HT-WGS reaction were determined at 330 °C, where the steady-state WGS conversions at 330 °C were kept between 1–9% in order to minimize transport limitations. The TOF values were determined by dividing the WGS catalytic activity by the number of catalytic active sites (Ns) that were determined from isotope switch experiments described in Section 2.6.

Table 1
BET surface areas of MO_x-Fe_2O_3 and CuO/MO_x-Fe_2O_3 catalysts. The used catalysts were treated under HT-WGS reaction conditions at 500 °C for 2 and 5 hours, respectively.

Sample	Composition (wt.%)	BET Surface Area (m^2/g)		
		Fresh	Used-2 h	Used-5 h
Si-Fe	8% SiO_2-92% Fe_2O_3	162	52	44
Cu/Si-Fe	2.9% CuO-7.8% SiO_2-89.3% Fe_2O_3	159	50	40
Mg-Fe	8% MgO-92% Fe_2O_3	130	36	29
Cu/Mg-Fe	2.9% CuO-7.8% MgO-89.3% Fe_2O_3	119	35	23
Al-Fe	8% Al_2O_3-92% Fe_2O_3	113	46	42
Cu/Al-Fe	2.9% CuO-7.8% Al_2O_3-89.3% Fe_2O_3	104	41	35
Cr-Fe	8% Cr_2O_3-92% Fe_2O_3	101	45	41
Cu/Cr-Fe	2.9% CuO-7.8% Cr_2O_3-89.3% Fe_2O_3	87	39	34

2.8. CO-temperature programmed reduction (TPR)

The CO-TPR experiments were carried out using an Altamira Instruments system (AMI-200). Approximately 30 mg of catalysts were first dehydrated under flowing 10% O_2/Ar at 350 °C for 1 hour followed by activation *via* HT-WGS reaction (10 ml/min 10% CO/Ar, 30 ml/min He flow through bubbler at 25 °C) at 350 °C for 90 min. After the catalyst was activated, the reactor was flushed by He and then cooled down to 80 °C. The CO-TPR experiments were then performed by ramping up the temperature under 10% CO/Ar at a rate of 10 °C/min.

3. Results

3.1. BET surface area

The BET surface areas of fresh and activated catalysts are listed in Table 1. Among the fresh non-Cu binary catalysts, Si-Fe exhibits the highest surface area of 162 m^2/g, followed by Mg-Fe (130 m^2/g), and Al-Fe (113 m^2/g) which are all larger than the fresh Cr-Fe (101 m^2/g) catalyst. Adding CuO slightly decreases the surface areas (~2–14%) with the greatest decrease observed for supported Cu/Cr-Fe catalyst.

To evaluate the thermostability of the catalysts under working condition, catalysts were treated at 500 °C under HT-WGS reaction condition for 2 and 5 h, respectively. The higher temperature than normal operating condition is to accelerate catalyst sintering. The BET surface areas were then directly measured without exposing the activated pyrophoric catalysts to air which might alter their surface morphology. All the catalysts showed significant decrease in the BET surface area, by ~60–80%, after high temperature treatment (Table 1). The Si-promoted catalysts exhibited the best thermostability (40–44 m^2/g) followed closely by the Cr (34–41 m^2/g) and Al (35–42 m^2/g) promoted catalysts. The Mg promoted catalysts, however, had the poorest thermostability with the lowest BET surface areas after the HT-WGS reaction (23–29 m^2/g).

3.2. XRD

The bulk phases of the fresh catalysts were characterized by XRD diffractograms under ambient conditions with only hematite phase observed (Fig. 1) [31]. The lack of any other phases from XRD patterns, however, doesn't exclude the existence of separate MO_x crystallites due to the size detection limitation of XRD technique (< 3 nm), low concentration of MO_x promoters or similarity of their lattice parameters. Thus, we specifically compared the hematite (1 1 0) main peak of MO_x-Fe_2O_3 with un-promoted Fe_2O_3 (Fig. 1c) to determine whether a solid solution is formed between MO_x and Fe_2O_3. The addition of promoters caused slight shift of the XRD hematite peak and their 2Θ positions follow the order of Al-Fe (36.05) > Cr-Fe (35.91) > Fe_2O_3 (35.85) ≈ Si-Fe (35.80) > Mg-Fe (35.67). This order, except Si-Fe, perfectly matches the trends of their ionic radii: Al^{3+} (0.535 Å) < Cr^{3+} (0.615 Å) < Fe^{3+} (0.645 Å) < Mg^{2+} (0.72 Å), indicating the Mg, Al and Cr promoters form solid solutions with Fe_2O_3. The SiO_2 promoter doesn't form a solid solution with Fe_2O_3 since the 2Θ value should be much higher than 36.05 (ionic radii of Si^{4+} is 0.4 Å) if a solid solution was dominant. It is not apparent from XRD if CuO forms a solid solution with MO_x-Fe_2O_3 due to its less concentration (Fig. S1).

3.3. In situ Raman spectrum

The *in situ* Raman spectra of the supported CuO/MO_x-Fe_2O_3 catalysts are presented in Fig. 2 as a function of environmental conditions. The Raman spectra of the initial dehydrated Cu-supported iron mixed oxide at 400 °C are presented in Fig. 2(a), and exhibit Raman bands at 585, 491, 389, 271 and 208 cm^{-1} that are characteristic of the bulk α-Fe_2O_3 phase [32]. The supported CuO/MgO-Fe_2O_3 and CuO/Al_2O_3-Fe_2O_3 catalysts possess a strong Raman band at 680 cm^{-1} that arises from photon scattering which indicates the formation of mixed-metal oxide solid solution [33]. The intensity of this 680 cm^{-1} band for supported CuO/Cr_2O_3-Fe_2O_3 is relatively lower, since only a portion of Cr species exist in the bulk and the majority present as surface dioxo $(O{=})_2CrO_2$ with Raman signature bands at 839 cm^{-1} (bridging Cr—O—Fe stretch) and 1000 cm^{-1} (symmetric O=Cr=O stretch) [34]. The supported CuO/SiO_2-Fe_2O_3 catalyst exhibits almost no 680 cm^{-1} band, which is consistent with XRD result that Si does not form a bulk solid solution with iron oxide.

Under the reverse water-gas shift (RWGS) reaction conditions at 400 °C, the bulk crystalline α-Fe_2O_3 (hematite) phase reduces and transforms to the bulk crystalline Fe_3O_4 (magnetite) phase (characteristic Raman bands at 282, 498 and 634 cm^{-1}) as presented in Fig. 2b [33]. The initially fully oxidized surface Cr^{6+} species reduces to Cr^{+3} during the RWGS reaction and dissolve into the bulk iron oxide lattice to form $Fe_{3-x}Cr_xO_4$ as indicated by the absence of Raman bands from the surface Cr—O—Fe and O=Cr=O vibrations [13]. Raman bands from Cu species are not observed under both dehydrated and reaction conditions and is related to the small concentration and lower Raman cross-section of CuO_x in the oxidized catalysts and metallic Cu in the activated catalyst relative to the greater amounts and higher Raman cross-sections of iron oxides [35].

3.4. HS-LEIS

To characterize the surface structure of CuO/MO_x-Fe_2O_3 catalysts with High Sensitivity – Low Energy Ion Scattering (HS-LEIS) spectroscopy, two types of probing ions were used: He^+ ions to resolve lighter elements such as O, Al, Mg and Si and Ne^+ ions to resolve heavier elements such as Cr, Fe and Cu.

The HS-LEIS spectra with He^+ as probing source for all catalysts are shown in Fig. 3. A dose amount of 1×10^{15} ions/cm^2 corresponds to the depth of one atomic layer [30]. The fresh CuO/Cr_2O_3-Fe_2O_3 catalyst shows a constant O peak at 1160 eV, an increasing peak at 2260 eV for Fe and Cr and a shoulder at 2360 eV representing Cu (Fig. 3a). After the catalyst is activated under RWGS condition, Na and K contaminants were observed, which also exist on all other three activated catalysts (Fig. 3b, d, f, h) and are likely to be introduced from the sample holder in the process of high temperature pre-treatment. The fresh CuO/Al_2O_3-Fe_2O_3 catalyst (Fig. 3c) exhibits a constant Al signal at 1730 eV, indicating that Al is evenly distributed. After activation, the intensity of Al is initially low and gradually increases to a constant value, meaning it is partially covered by surface oxides. Similarly, the Mg signal (1600 eV) for fresh CuO/MgO-Fe_2O_3 catalyst stays constant upon sputtering and is consistent with Raman and XRD results. After activation, the Mg signal (Fig. 3f) merged with the Na contamination peak preventing its monitoring with He^+ ions. It's however reasonable to compare the intensity of this 1600 eV peak with those from other activated catalysts. The higher and constant 1600 eV for CuO/MgO-Fe_2O_3 suggests that Mg is also homogeneously distributed after activation.

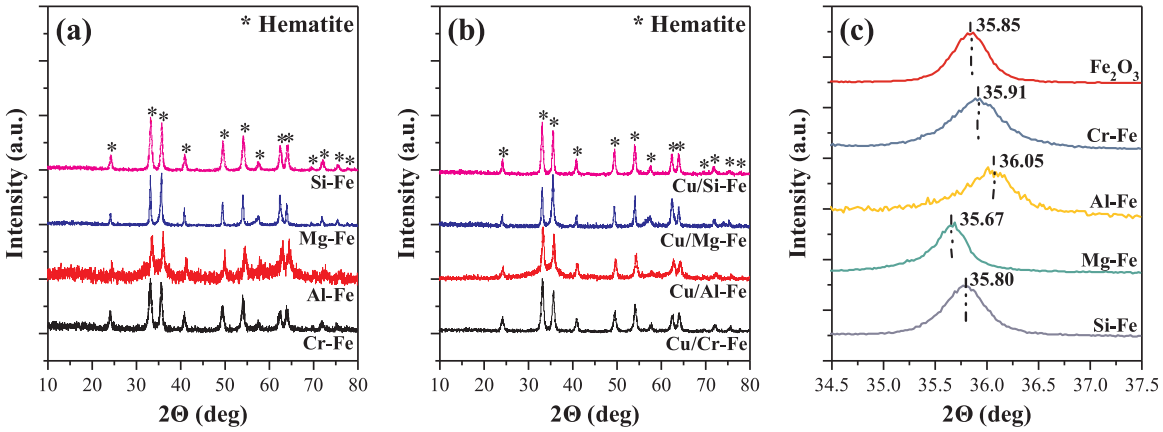

Fig. 1. XRD diffractograms of fresh calcined catalysts. (a) full scan of MO_x-Fe_2O_3, (b) full scan of CuO/MO_x-Fe_2O_3 and (c) main XRD peak of hematite (1 1 0) of the fresh calcined Fe_2O_3 and MO_x-Fe_2O_3 catalysts. (M = Si, Mg, Al or Cr). * represents the XRD peaks of the hematite phase.

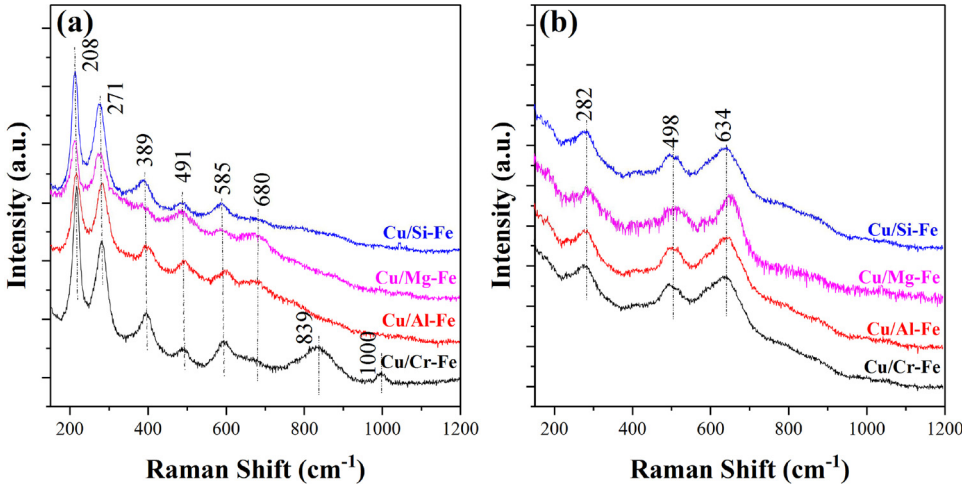

Fig. 2. *In situ* Raman spectra of supported CuO/MO_x-Fe_2O_3 under (a) dehydrated conditions (T = 400 °C; 30 ml/min 10% O_2/Ar) and (b) RWGS reaction conditions (T = 400 °C; 10 ml/min CO_2, 10 ml/min H_2 and 10 ml/min Ar).

The fresh CuO/SiO_2-Fe_2O_3 catalyst (Fig. 3g) possesses a Si peak at 1860 eV that is only observable after the first layer is sputtered suggesting Si species (SiO_2 based on XRD and Raman results) are covered by a thin layer. Such an overlayer becomes thicker after activation since the Si signal is not observable as shown in Fig. 3h.

The Ne^+ ions were used as probe to study the distribution of copper in the CuO/MO_x-Fe_2O_3 catalysts before and after RWGS treatment. The Cr signal is also resolved with Ne^+ ions from the dominating Fe signal for the CuO/Cr_2O_3-Fe_2O_3 catalyst. In the fresh catalyst (Fig. 4a), the Cr was surface enriched as surface Cr^{6+} species, which reduce upon activation and migrate into the bulk lattice (Fig. 4b). For all catalysts, the intensity of Fe signal increases with sputtering depth due to the preferential sputtering of O atoms from iron oxide [36,37]. After the oxygen plasma treatments, the Cu signal at ~1425 eV increases upon sputtering and levels off after removal of 2–3 atomic layers, suggesting that copper species are somehow deficient at this region. After the catalysts were activated with CO_2 + H_2, the Cu species are known to reduce to metallic Cu particles [13,38]. The initially increasing HS-LEIS signal of Cu upon sputtering in Fig. 4b, d and h again demonstrates that these reduced Cu° are partially covered by some overlayer which is most likely to be FeO_x due to its strong metal support interaction [39]. The exception is for the CO_2 + H_2 treated CuO/MgO-Fe_2O_3 catalyst, where a very weak Cu signal is observed that slightly increases after a few sputter cycles. This suggests that reduced CuO/MgO-Fe_2O_3 catalyst possesses much larger copper nanoparticles than other catalysts.

3.5. Catalytic activity

The steady-state HT-WGS reaction rates for the MO_x-Fe_2O_3 mixed oxide and supported Cu/MO_x-Fe_2O_3 catalysts are presented in Fig. 5 as Arrhenius plots with detailed apparent activation energy values and pre-exponential factors shown in Table S1. The Cr_2O_3-Fe_2O_3 exhibits the highest HT-WGS activity among the tested binary MO_x-Fe_2O_3 catalysts, closely followed by Al_2O_3-Fe_2O_3 and MgO-Fe_2O_3, with the SiO_2-Fe_2O_3 mixed oxide catalyst shows the lowest activity. The apparent activation energies for the HT-WGS reaction were found to be ~101–123 kJ/mol. As a chemical promoter, CuO significantly improves the catalytic activity of all catalysts and decreases their activation energies to ~67–72 kJ/mol [13]. For the CuO promoted ternary catalysts, CuO/Al_2O_3-Fe_2O_3 and CuO/Cr_2O_3-Fe_2O_3 catalysts exhibit comparable HT-WGS activity, while the CuO/MgO-Fe_2O_3 is less active and the CuO/SiO_2-Fe_2O_3 is least active.

In addition to the apparent catalytic activities, we also sought to compare the intrinsic catalytic activity by determining their turnover frequency (TOF) values for the HT-WGS reaction at 330 °C. The number of participating redox oxygen atoms, Ns, were determined by the isotope switch method ($C^{16}O_2/H_2 \rightarrow C^{18}O_2/H_2$) that was previously developed [40]. The MO_x-Fe_2O_3 mixed oxide catalysts possess very similar Ns values (1.7–2.3 × 10^{-3} mol/g) as summarized in Table 2. Addition of the Cu promoter only has a slight effect on the number of active sites (1.7k2.0 × 10^{-3} mol/g). The TOF values were determined by dividing the WGS catalytic activity by the number of catalytic active sites (Ns)

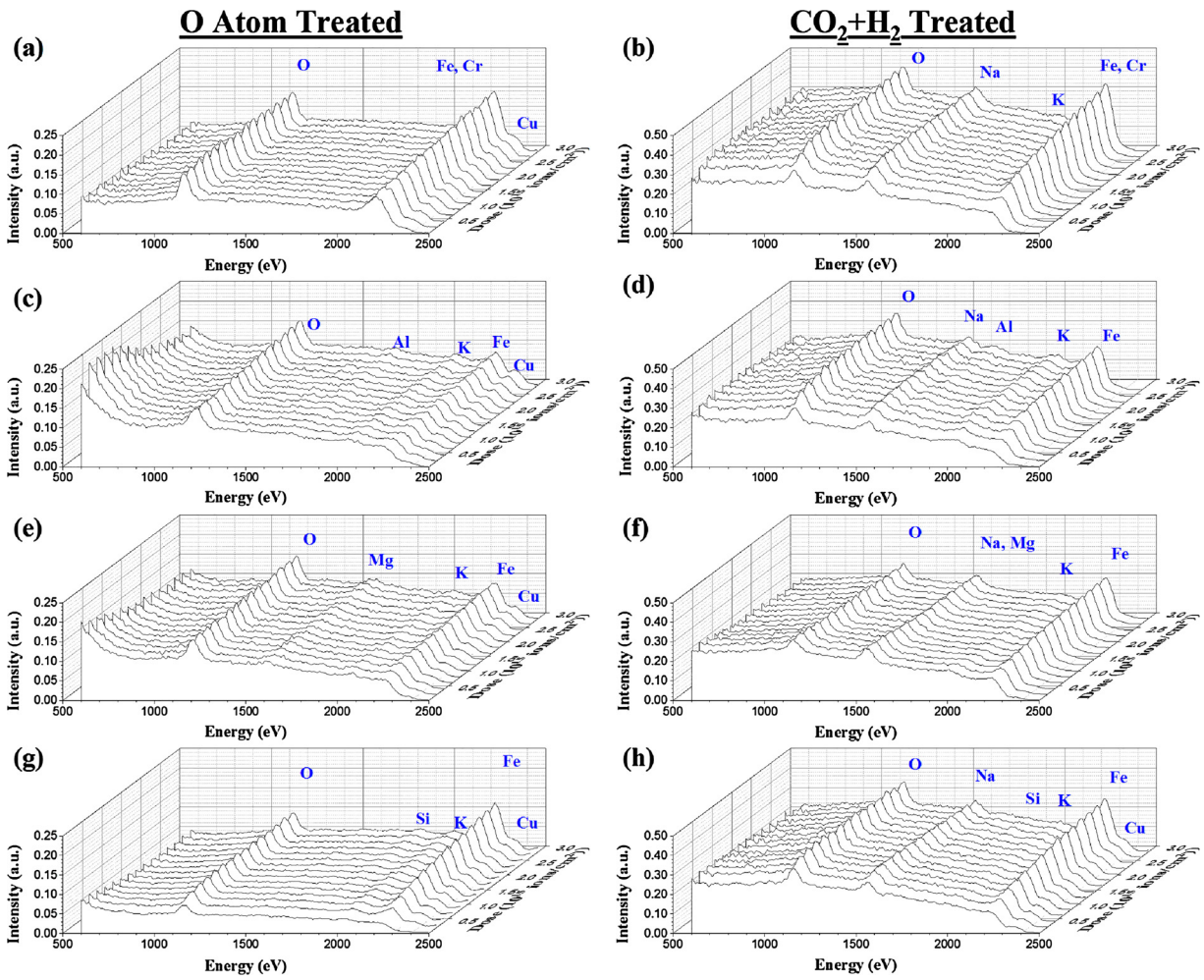

Fig. 3. HS-LEIS depth profile for (a, b) CuO/Cr_2O_3-Fe_2O_3, (c, d) CuO/Al_2O_3-Fe_2O_3, (e, f) CuO/MgO-Fe_2O_3 and (g, h) CuO/SiO_2-Fe_2O_3 after oxygen plasma treatment and CO_2+H_2 pretreatment respectively using He^+ ion as probe.

(Table 2). For the binary MO_x-Fe_2O_3 catalysts, the TOF values vary from 0.2×10^{-3}– $1.2 \times 10^{-3}\,s^{-1}$ and follow the order of Cr ~ Al > Mg > Si. The addition of Cu increases the TOF by ~3x, confirming its chemical promoting effect on the HT-WGS reaction [12]. The TOF values of the Cu-promoted ternary catalysts vary from 0.5×10^{-3}–$3.3 \times 10^{-3}\,s^{-1}$ with the order of Cr ~ Al > Mg > Si, which is the same as the binary catalysts.

3.6. CO-TPR

During the HT-WGS reaction, the reduction of surface oxygen by CO is involved in the rate-determining-step [41]. Thus, the redox characteristics of surface oxygen during the HT-WGS reaction directly correlates with the overall catalytic performance and was hereby evaluated by CO-TPR on activated catalysts (Fig. 6). The CO_2 peaks at 100–250 °C are assigned to the reduction of surface oxygen and the increasing signal after 300 °C are from the over-reduction of bulk Fe_3O_4 to FeO or even metallic Fe. The activated CuO/Cr_2O_3-Fe_2O_3 catalyst exhibits a surface reduction peak at 147 °C, which is close to previously reported CuO-Cr_2O_3-Fe_2O_3 mixed oxide catalyst [13]. CuO/Al_2O_3-Fe_2O_3 possesses a very similar reduction peak for surface oxygen (148 °C) to that of the Cr-promoted catalyst, demonstrating their similar activity of surface oxygen intermediates. The reduction of the surface oxygen species on the CuO/MgO-Fe_2O_3 catalyst is more sluggish and probably occurs at higher temperatures that overlap the reduction peak from the bulk. The CuO/SiO_2-Fe_2O_3 catalyst, which exhibited the lowest TOF, has a surface reduction peak at a higher temperature (179 °C), accordingly.

4. Discussion

4.1. Catalyst structure before and during WGS reaction

By combining the characterization results including XRD, *in situ* Raman, *in situ* HS-LEIS, and previously reported *in situ* Near Ambient Pressure (NAP) XPS measurements [13], structure of Cu promoted ternary catalysts can be depicted as shown in Scheme 1. For the initially oxidized CuO/Cr_2O_3-Fe_2O_3 catalyst (Scheme 1a), surface $Cr^{6+}O_x$ species are present on the surface layer with both CuO and $Cr^{3+}O_x$ forming bulk mixed oxide solutions with Fe_2O_3 (Raman and XRD) [13]. During the HT-WGS reaction, the catalyst bulk phase transforms to a $Fe_{3-x}Cr_xO_4$ mixed oxide solution. Simultaneously, Cu^{2+} is reduced to Cu° and forms small supported metallic nanoparticles that are partially covered by a FeO_x overlayer (HS-LEIS) [13]. The initial CuO/Al_2O_3-Fe_2O_3 catalyst (Scheme 1b) mainly exists as a mixed oxide solid solution of $Fe_{2-x-y}Al_xCu_yO_3$ before reaction, with the surface layers deficient in Cu (Raman, XRD and HS-LEIS). During the HT-WGS reaction, reduced Cu nanoparticles that are partially covered by an FeO_x overlayer are present on the bulk $Fe_{3-x}Al_xO_4$ mixed oxide (HS-LEIS). The fresh and activated CuO/MgO-Fe_2O_3 catalyst has a very similar structure to CuO/Al_2O_3-Fe_2O_3 with the exception of the much larger size of Cu nanoparticles during the reaction (Scheme 1c). This is because the Fe_3O_4-MgO mixture isn't as good in preventing the sintering of reduced copper particles, which is evident from its much lower BET surface area after

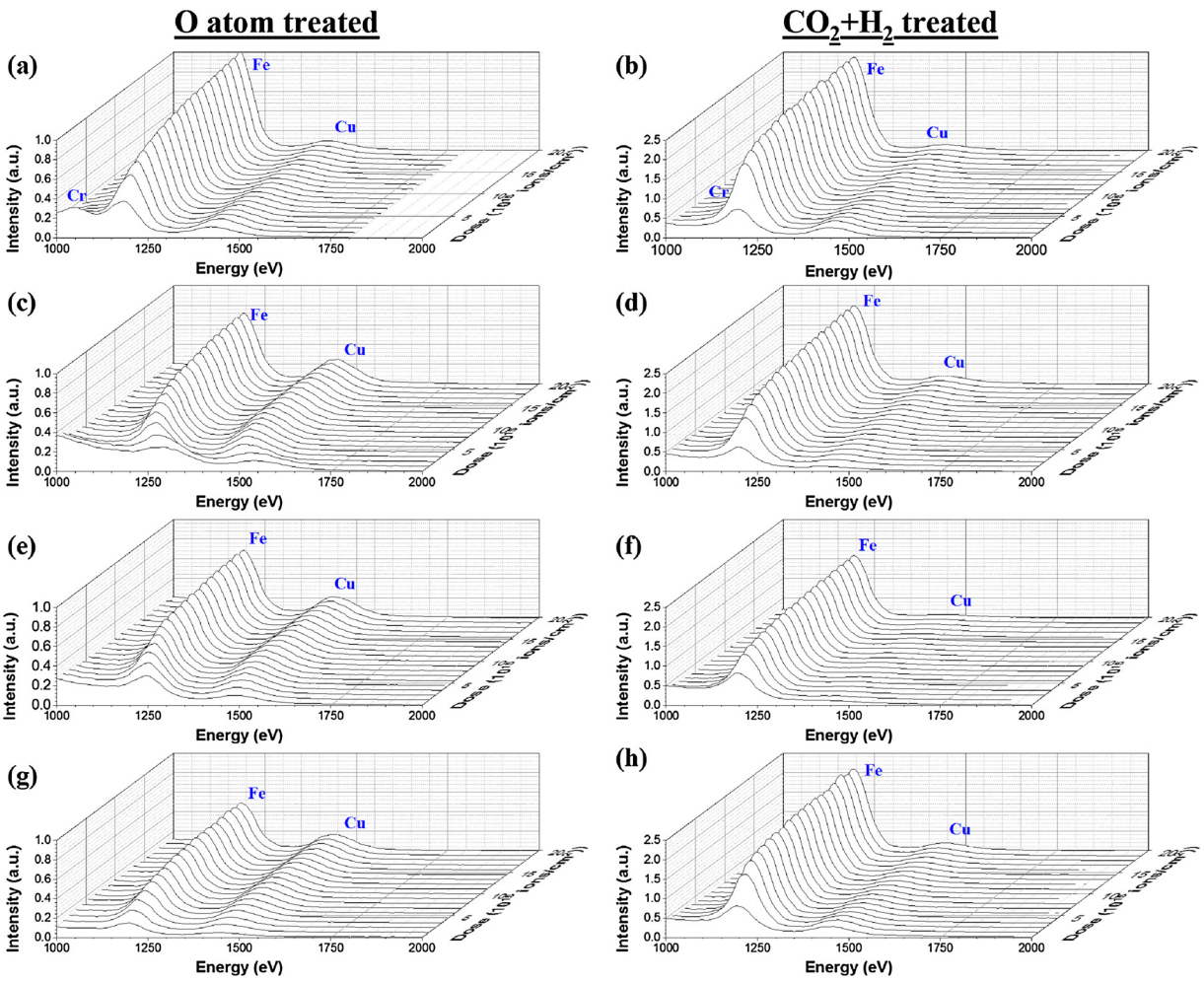

Fig. 4. HS-LEIS depth profile for (a, b) CuO/Cr_2O_3-Fe_2O_3, (c, d) CuO/Al_2O_3-Fe_2O_3, (e, f) CuO/MgO-Fe_2O_3 and (g, h) CuO/SiO_2-Fe_2O_3 after oxygen plasma treatment and CO_2 + H_2 pretreatment respectively using Ne^+ ion as probe.

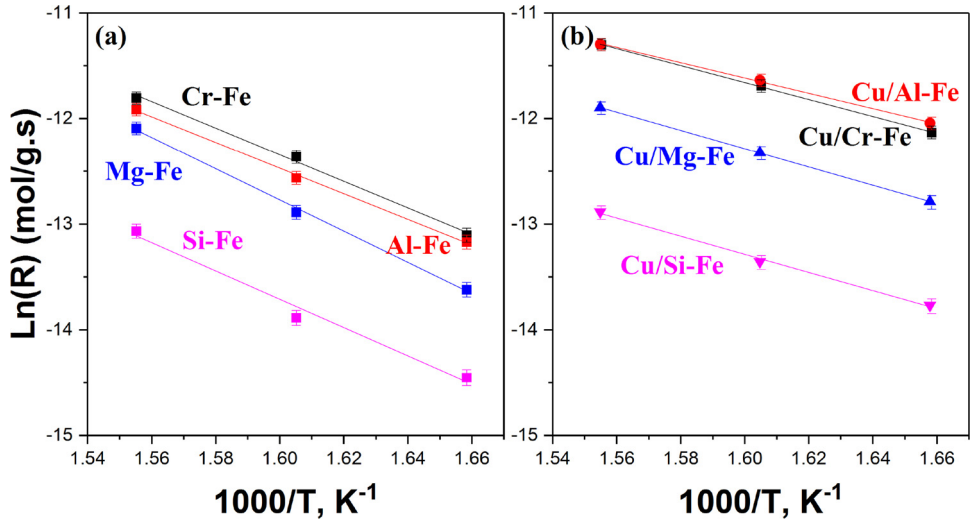

Fig. 5. Arrhenius plots for steady-state WGS reaction rates for (a) MO_x-Fe_2O_3 mixed oxide catalysts; (b) supported CuO/MO_x-Fe_2O_3 catalysts.

reaction. The initial oxidized structure of the CuO/SiO_2-Fe_2O_3 catalyst is different from the other three catalysts since SiO_2 doesn't form a solid solution with Fe_2O_3 (Raman, XRD and HS-LEIS). It's likely that a core-shell structure is formed between SiO_2 and some portion of Fe_2O_3-CuO (Scheme 1d). Upon activation by the WGS reaction conditions, the SiO_2 nanoparticles seem to become encapsulated by a much thicker Fe_3O_4 overlayer due to the sintering effect. The reduced Cu nanoparticles migrated towards the surface and are partially covered by an FeO_x overlayer (HS-LEIS).

Table 2
WGS activity, number of sites, and turnover frequencies (TOFs). (10% CO/Ar (10 ml/min), He (30 ml/min) and water vapor (H_2O/CO ~1); T = 330 °C).

Catalyst	Amount (mg)	CO conversion (%)	CO consumption rate (10^{-6} mol/s·g)	Ns[a] (10^{-3} mol/g)	TOF (10^{-3} s^{-1})
Cr-Fe	12.5	3.8	2.0	1.7	1.2
Cu/Cr-Fe	10.3	8.8	5.4	1.7	3.3
Al-Fe	10.2	2.9	1.9	1.9	1.0
Cu/Al-Fe	10.3	9.0	5.9	1.8	3.2
Mg-Fe	10.1	1.8	1.2	2.3	0.5
Cu/Mg-Fe	10.8	4.5	2.8	2.0	1.4
Si-Fe	14.2	1.1	0.5	2.3	0.2
Cu/Si-Fe	10.1	1.6	1.0	1.9	0.5

[a] Ns, number of participating redox oxygen atoms [40].

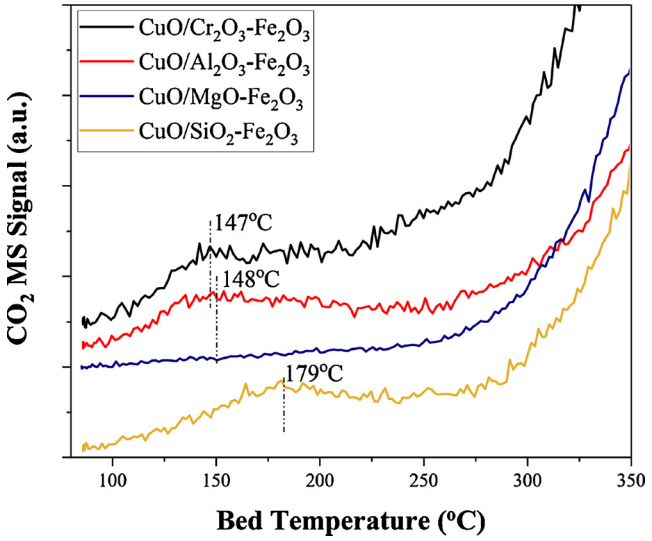

Fig. 6. CO-TPR profile of activated CuO/MO_x-Fe (M = Cr, Al, Mg and Si) catalysts.

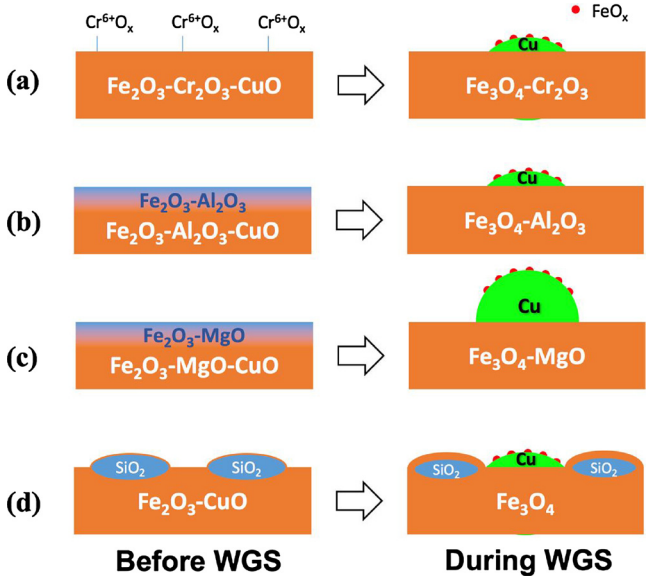

Scheme 1. Structures of (a) CuO/Cr_2O_3-Fe_2O_3, (b) CuO/Al_2O_3-Fe_2O_3, (c) CuO/MgO-Fe_2O_3 and (d) CuO/SiO_2-Fe_2O_3 before (left) and during the WGS reaction (right).

4.2. Structure-activity relationship

The catalyst structure during reaction, together with their catalytic performance, has allowed elucidating the structure-activity relationships of the Cr-free HT-WGS catalysts promoted with Al, Mg and Si. CuO/Al_2O_3-Fe_2O_3 catalyst, which has received the most attention in the literature, shows similar morphology to the commercial-type CuO/Cr_2O_3-Fe_2O_3 catalyst in terms of both surface structure and particle size. More importantly, the similar dimension of Cu nanoparticles during the reaction that's verified by HS-LEIS results in a comparable amount of Cu-Fe_3O_4 interface. This metal-metal oxide interface is known to play a key role in HT-WGS reaction and be more active than Cu and Fe_3O_4 alone [13,42,43]. As a result, the Al promoted catalysts exhibited almost the same TOF with Cr-promoted catalysts.

Although Mg promoted CuO/MgO-Fe_2O_3 catalyst also has a similar morphology with Cr and Al promoted catalysts, its much lower surface area hampered the overall apparent catalytic activity. In addition, the poor stabilization ability of Mg has rendered much larger Cu nanoparticles with negligible Cu-Fe_3O_4 interface. This also explains the absence of clear reduction peak for surface oxygen at the low temperature region that's observed for other three ternary catalysts. Si is another "bad" promoter with much lower TOF compared to Cr. Regardless of its incompatibility into Fe_2O_3 and Fe_3O_4 lattice, the SiO_2 can prevent the iron oxides and copper nanoparticles from sintering, probably by functioning as a support. However, compared to the Cr promoter, Si has a negative impact on the reducibility of surface oxygen atom during the reaction with a much higher reduction T_p observed (179 °C *vs.* 147 °C), which explains the much lower TOF.

5. Conclusions

We demonstrate, with a series *in situ* characterization and catalytic performance evaluation, the structure-activity relationships of non-Cr ternary CuO/MO_x-Fe_2O_3 catalysts promoted by three earth abundant elements (Al, Mg and Si). Unlike Cr that's surface enriched in fresh catalysts due to the existence of surface Cr^{6+} species, Al and Mg are distributed within the bulk lattice of both fresh and activated catalysts, functioning as texture promoters. The SiO_2 promoter in both fresh and activated catalysts exists as discrete SiO_2 nanoparticles that are covered by an iron oxide overlayer. The Mg promoter's poor thermostability at HT-WGS condition significantly suppressed the amount of Cu-Fe_3O_4 interface, resulting in a low TOF. The SiO_2 promoted catalyst was found to yield the best thermostability under HT-WGS, but lowest TOF value due to its negative impact on reducibility of surface oxygen during reaction compared to Cr_2O_3 promoted catalyst. The Al promoted catalyst was found to exhibit comparable thermostability and TOF to the conventional Cr-containing catalysts (both Cu-free and supported Cu) making Al_2O_3 the best substitute for Cr-free HT-WGS supported Cu/iron oxide catalysts.

Acknowledgments

The authors acknowledge financial support from National Science Foundation Grant CBET – 1511689. Dr. Henry Luftman of Lehigh University is thanked for assisting with the collection of the HS-LEIS data. Özgen Yalçın gratefully acknowledges TUBITAK (The Scientific and Technology Research Council of Turkey) for financial support through 2214/B International Joint Ph.D. Fellowship Programme.

Appendix A. Supplementary data

Supplementary material related to this article can be found, in the online version, at doi:https://doi.org/10.1016/j.apcatb.2018.03.051.

References

[1] D.S. Newsome, The water-gas shift reaction, Catal. Rev. 21 (1980) 275–318, http://dx.doi.org/10.1080/03602458008067535.

[2] C. Ratnasamy, J.P. Wagner, Water gas shift catalysis, Catal. Rev. 51 (2009) 325–440, http://dx.doi.org/10.1080/01614940903048661.

[3] A. Chakrabarti, M.E. Ford, D. Gregory, R. Hu, C.J. Keturakis, S. Lwin, Y. Tang, Z. Yang, M. Zhu, M.A. Bañares, I.E. Wachs, A decade+ of operando spectroscopy studies, Catal. Today 283 (2017) 27–53, http://dx.doi.org/10.1016/j.cattod.2016.12.012.

[4] M.L. Kundu, A.C. Sengupta, G.C. Maiti, B. Sen, S.K. Ghosh, V.I. Kuznetsov, G.N. Kustova, E.N. Yurchenko, Characterization of chromia-promoted gamma-iron oxide catalysts and their CO conversion efficiency, J. Catal. 112 (1988) 375–383, http://dx.doi.org/10.1016/0021-9517(88)90151-0.

[5] A. Patlolla, E.V. Carino, S.N. Ehrlich, E. Stavitski, A.I. Frenkel, Application of operando XAS, XRD, and Raman spectroscopy for phase speciation in water gas shift reaction catalysts, ACS Catal. 2 (2012) 2216–2223, http://dx.doi.org/10.1021/cs300414c.

[6] M. Zhu, I.E. Wachs, A perspective on chromium-free iron oxide-based catalysts for high temperature water-gas shift reaction, Catal. Today (2017), http://dx.doi.org/10.1016/j.cattod.2017.08.042 available at: https://www.sciencedirect.com/science/article/pii/S0920586117305643.

[7] C.J. Keturakis, M. Zhu, E.K. Gibson, M. Daturi, F. Tao, A.I. Frenkel, I.E. Wachs, Dynamics of CrO3-Fe2O3 catalysts during the high-temperature water-gas shift reaction: molecular structures and reactivity, ACS Catal. 6 (2016) 4786–4798, http://dx.doi.org/10.1021/acscatal.6b01281.

[8] A. Andreev, V. Idakiev, D. Mihajlova, D. Shopov, Iron-based catalysts for the water gas shift reaction promoted by first row transition metals, Appl. Catal. A: Gen. 22 (1986) 385–387.

[9] V. Idakiev, D. Mihajlova, B. Kunev, A. Andreev, Effect of copper oxide on the catalytic activity of iron-chromia catalyst for water gas shift reaction, React. Kinet. Catal. Lett. 33 (1987) 119–124, http://dx.doi.org/10.1007/BF02066710.

[10] G.K. Reddy, K. Gunasekera, P. Boolchand, J. Dong, P.G. Smirniotis, High temperature water gas shift reaction over nanocrystalline copper codoped-modified ferrites, J. Phys. Chem. C (2011) 7586–7595, http://dx.doi.org/10.1021/jp2003084.

[11] G.K. Reddy, P. Boolchand, P.G. Smirniotis, Unexpected behavior of copper in modified ferrites during high temperature WGS reaction-aspects of Fe3+ ↔ Fe2 + redox chemistry from Mossbauer and XPS studies, J. Phys. Chem. C 116 (2012) 11019–11031, http://dx.doi.org/10.1021/jp301090d.

[12] S.M. Latifi, A. Salehirad, High temperature water gas shift reaction over Fe-Cr-Cu nanocatalyst fabricated by a novel method, Korean J. Chem. Eng. 33 (2016) 473–480, http://dx.doi.org/10.1007/s11814-015-0138-3.

[13] M. Zhu, T.C.R. Rocha, T. Lunkenbein, A. Knop-Gericke, R. Schlögl, I.E. Wachs, Promotion mechanisms of iron oxide-based high temperature water–gas shift catalysts by chromium and copper, ACS Catal. 6 (2016) 4455–4464, http://dx.doi.org/10.1021/acscatal.6b00698.

[14] C. Pellerin, S.M. Booker, Reflections on hexavalent chromium: health hazards of an industrial heavyweight, Environ. Health Perspect. 108 (2000) a402–a407, http://dx.doi.org/10.1289/ehp.108-a402.

[15] D.G. Rethwisch, J.A. Dumesic, The effects of metal-oxygen bond strength on properties of oxides: II. Water-gas shift over bulk oxides, Appl. Catal. 21 (1986) 97–109, http://dx.doi.org/10.1016/S0166-9834(00)81331-7.

[16] G.C. Chinchen, Catalytic preparation of hydrogen from carbon monoxide and water, EP 0062410 A1 (1982).

[17] J.Y. Lee, D.W. Lee, Y.K. Hong, K.Y. Lee, The CO removal performances of Cr-free Fe/Ni catalysts for high temperature WGSR under LNG reformate condition without additional steam, Int. J. Hydrogen Energy 36 (2011) 8173–8180, http://dx.doi.org/10.1016/j.ijhydene.2011.03.164.

[18] J.Y. Lee, D.-W. Lee, K.-Y. Lee, Y. Wang, Cr-free Fe-based metal oxide catalysts for high temperature water gas shift reaction of fuel processor using LPG, Catal. Today 146 (2009) 260–264, http://dx.doi.org/10.1016/j.cattod.2009.01.041.

[19] J.Y. Lee, D.W. Lee, M.S. Lee, K.Y. Lee, Cs-promoted Ni/Fe catalyst as a Cr-free, high temperature shift catalyst for steam methane reformate without additional supply of steam, Catal. Commun. 15 (2011) 37–40, http://dx.doi.org/10.1016/j.catcom.2011.08.010.

[20] F. Meshkani, M. Rezaei, Promoted Fe2O3-Al2O3-CuO chromium-free catalysts for high-temperature water-gas shift reaction, Chem. Eng. Technol. 38 (2015) 1380–1386, http://dx.doi.org/10.1002/ceat.201400668.

[21] F. Meshkani, M. Rezaei, High-temperature water-gas shift reaction over nanostructured Cr-free Fe2O3-Al2O3-CuO-MO (M: Ba, Ca, Mg and Sr) catalysts for hydrogen production, J. Ind. Eng. Chem. 30 (2015) 353–358, http://dx.doi.org/10.1016/j.jiec.2015.05.039.

[22] F. Meshkani, M. Rezaei, Preparation of mesoporous nanocrystalline alkali promoted chromium free catalysts (Fe2O3–Al2O3–NiO) for a high temperature water gas shift reaction, RSC Adv. 5 (2015) 9955–9964, http://dx.doi.org/10.1039/C4RA13508C.

[23] G.C. de Araújo, M. do Carmo Rangel, An environmental friendly dopant for the high-temperature shift catalysts, Catal. Today 62 (2000) 201–207, http://dx.doi.org/10.1016/S0920-5861(00)00421-1.

[24] Q. Liu, W. Ma, R. He, Z. Mu, Reaction and characterization studies of an industrial Cr-free iron-based catalyst for high-temperature water gas shift reaction, Catal. Today 106 (2005) 52–56, http://dx.doi.org/10.1016/j.cattod.2005.07.150.

[25] J.M.T. de Souza, M. do Carmo Rangel, Aluminium-doped catalysts for the high temperature shift reaction, React. Kinet. Catal. Lett. 77 (2002) 29–34, http://dx.doi.org/10.1023/A:1020379400569.

[26] A.O. de Souza, M. do Carmo Rangel, Catalytic activity of aluminium and copper-doped magnetite in the high temperature shift reaction, React. Kinet. Catal. Lett. 79 (2003) 175–180, http://dx.doi.org/10.1023/A:1024132406523.

[27] J.M.T. de Souza, M. do Carmo Rangel, Catalytic activity of aluminium-rich hematite in the water gas shift reaction, React. Kinet. Catal. Lett. 83 (2004) 93–98, http://dx.doi.org/10.1023/B:REAC.0000037381.72220.66.

[28] A. Khan, P. Chen, P. Boolchand, P.G. Smirniotis, Modified nano-crystalline ferrites for high-temperature WGS membrane reactor applications, J. Catal. 253 (2008) 91–104, http://dx.doi.org/10.1016/j.jcat.2007.10.018.

[29] F. Meshkani, M. Rezaei, M. Jafarbegloo, Applying Taguchi robust design to the optimization of the synthesis parameters of nanocrystalline Cr-free Fe-Al-Cu catalyst for high temperature water gas shift reaction, Mater. Res. Bull. 70 (2015) 229–235, http://dx.doi.org/10.1016/j.materresbull.2015.04.030.

[30] S.P. Phivilay, A.A. Puretzky, K. Domen, I.E. Wachs, Nature of catalytic active sites present on the surface of advanced bulk tantalum mixed oxide photocatalysts, ACS Catal. 3 (2013) 2920–2929, http://dx.doi.org/10.1021/cs400662m.

[31] I.S. Lyubutin, C.R. Lin, Y.V. Korzhetskiy, T.V. Dmitrieva, R.K. Chiang, Mössbauer spectroscopy and magnetic properties of hematite/magnetite nanocomposites, J. Appl. Phys. 106 (2009), http://dx.doi.org/10.1063/1.3194316.

[32] J.M. Jehng, I.E. Wachs, F.T. Clark, M.C. Springman, Raman characterization of alumina supported MoVFe catalysts: influence of calcination temperature, J. Mol. Catal. 81 (1993) 63–75, http://dx.doi.org/10.1016/0304-5102(93)80023-N.

[33] K.F. McCarty, D.R. Boehme, A Raman study of the systems Fe3-xCrxO4 and Fe2-xCrxO3, J. Solid State Chem. 79 (1989) 19–27, http://dx.doi.org/10.1016/0022-4596(89)90245-4.

[34] E.L. Lee, I.E. Wachs, In situ spectroscopic investigation of the molecular and electronic structures of SiO2 supported surface metal oxides, J. Phys. Chem. C 111 (2007) 14410–14425, http://dx.doi.org/10.1021/jp0735482.

[35] M. Kilo, C. Schild, A. Wokaun, A. Baiker, Surface oxidic phases of binary and ternary zirconia-supported metal catalysts investigated by Raman spectroscopy, J. Chem. Soc. Faraday Trans. 88 (1992) 1453, http://dx.doi.org/10.1039/ft9928801453.

[36] M.R. Anantharaman, S. Reijne, J.P. Jacobs, H.H. Brongersma, R.H.H. Smits, K. Seshan, Preferential exposure of certain crystallographic planes on the surface of spinel ferrites: a study by LEIS on polycrystalline spinel ferrite surfaces, J. Mater. Sci. 34 (1999) 4279–4283, http://dx.doi.org/10.1023/A:1004615222119.

[37] M. de Ridder, P.C. van de Ven, R.G. van Welzenis, H.H. Brongersma, S. Helfensteyn, C. Creemers, P. Van Der Voort, M. Baltes, M. Mathieu, E.F. Vansant, Growth of iron oxide on yttria-stabilized zirconia by atomic layer deposition, J. Phys. Chem. B 106 (2002) 13146–13153, http://dx.doi.org/10.1021/jp0211640.

[38] Y. Ye, L. Wang, S. Zhang, Y. Zhu, J. Shan, F. (Feng) Tao, The role of copper in catalytic performance of a Fe–Cu–Al–O catalyst for water gas shift reaction, Chem. Commun. 49 (2013) 4385, http://dx.doi.org/10.1039/c2cc37416a.

[39] R. Naumann d'Alnoncourt, M. Friedrich, E. Kunkes, D. Rosenthal, F. Girgsdies, B. Zhang, L. Shao, M. Schuster, M. Behrens, R. Schlögl, Strong metal–support interactions between palladium and iron oxide and their effect on CO oxidation, J. Catal. 317 (2014) 220–228, http://dx.doi.org/10.1016/j.jcat.2014.06.019.

[40] M. Zhu, I.E. Wachs, Determining number of active sites and TOF for the high-temperature water gas shift reaction by iron oxide-based catalysts, ACS Catal. 6 (2016) 1764–1767, http://dx.doi.org/10.1021/acscatal.5b02961.

[41] M. Zhu, I.E. Wachs, Resolving the reaction mechanism for H2 formation from high-temperature water–gas shift by chromium–iron oxide catalysts, ACS Catal. 6 (2016) 2827–2830, http://dx.doi.org/10.1021/acscatal.6b00659.

[42] C.S. Chen, W.H. Cheng, S.S. Lin, Enhanced activity and stability of a Cu/SiO2 catalyst for the reverse water gas shift reaction by an iron promoter, Chem. Commun. (Camb.) (2001) 1770–1771, http://dx.doi.org/10.1039/b104279n.

[43] C.S. Chen, W.H. Cheng, S.S. Lin, Study of iron-promoted Cu/SiO2 catalyst on high temperature reverse water gas shift reaction, Appl. Catal. A: Gen. 257 (2004) 97–106, http://dx.doi.org/10.1016/S0926-860X(03)00637-9.